CHEMISTRY
A EUROPEAN JOURNAL

DOI: 10.1002/chem.200701822

Controllable Synthesis of VSB-5 Microspheres and Microrods: Growth Mechanism and Selective Hydrogenation Catalysis

Shu-Juan Liu,[a] Hai-Yang Cheng,[b] Feng-Yu Zhao,[b] Jun-Yan Gong,[a] and Shu-Hong Yu*[a]

Abstract: Nanoporous VSB-5 nickel phosphate molecular sieves with relatively well controllable sizes and morphology of microspheres assembled from nanorods were synthesized at 140 °C over a short time in the presence of hexamethylenetetramine (HMT) by a facile hydrothermal method. The pH value, reaction time, and ratio of HMT to $NaHPO_2 \cdot H_2O$ crucially influence the morphology and quality of the final products. By adjusting the pH value of the initial reaction solution, the morphology changes from disperse rods to microspheres assembled from rods and finally to a large quantity of fibers, and the diameters of the VSB-5 rods can be varied. The catalytic activity of VSB-5 in selective hydrogenation of several unsaturated organic compounds was tested. Nickel(II) in VSB-5 can selectively catalyze hydrogenation of C=C in *trans*-cinnamaldehyde and 3-methylcrotonaldehyde. In addition, since nitrobenzene (NB) and 2-chloronitrobenzene could be reduced to aniline (AN) and 2-chloroaniline with high selectivity, VSB-5 could have potential applications in synthesizing dyes, agrochemicals, and pharmaceuticals.

Keywords: heterogeneous catalysis · hydrogenation · hydrothermal synthesis · nanoporous materials · nickel

Introduction

As important intermediates for dyes, urethanes, agrochemicals, and pharmaceuticals, chloroanilines are commonly prepared by selective hydrogenation of nitro compounds.[1] However, besides the chloroaniline main product, several intermediates and side products, such as nitrobenzene (NB), aniline (AN), azoxybenzene (AOB), azobenzene (AB), and hydrazobenzene (HOB), have also been reported.[2] Selective hydrogenation of α,β-unsaturated aldehydes, which would have great significance for the production of fine chemicals, especially for use in the fragrance and flavor industry,[3,4] suffers from the same problem. Thus, increasing efforts have been devoted to searching for new catalysts with outstanding catalytic performance. In general, they can be divided into two categories: single metals such as Pd, Pt, Ru, or Ni supported on materials like MCM-41, α-alumina, and SiO_2,[5] and alloys (e.g., NiB, CoB, NiP) or bimetallic compounds (Ni–Cu, Ru–Cu, etc.).[6] Most nickel catalysts for selective hydrogenation consist of Ni^0 loaded on a support, or framework Ni^{II} is reduced to Ni^0.[7] Until now, few investigations on selective hydrogenation with unreduced Ni^{II} catalysts have been reported.

As a newly emerging nanoporous material with open framework, the nickel phosphate VSB-5, which has outstanding properties such as high BET surface area, ion-exchange capability, and shape-selective catalysis with high thermal stability, has aroused considerable attention. In contrast to traditional aluminosilicate zeolites, the different valences and various coordination numbers of the nickel ions make VSB-5 one of the most promising materials for applications in optical, electronic, and magnetic fields. Guillou et al.[8] concluded that Ni exists as Ni^{II} in VSB-5, and they also studied the catalytic activity of reduced VSB-5 in selective hydrogenation of 1,3-butadiene. Before being used in hydrogenation, VSB-5 was activated in H_2 at 350 °C for several hours, and the conversion rate of 1,3-butadiene increased with increasing activation time. From this point of

[a] S.-J. Liu, J.-Y. Gong, Prof. Dr. S.-H. Yu
Division of Nanomaterials & Chemistry
Hefei National Laboratory for Physical Sciences at Microscale
Structural Research Laboratory of CAS
Department of Materials Science and Engineering
University of Science and Technology of China
Hefei 230026 (China)
Fax: (+86) 0551-3603040
E-mail: shyu@ustc.edu.cn

[b] H.-Y. Cheng, Prof. Dr. F.-Y. Zhao
State Key laboratory of Electroanalytical Chemistry
Changchun Institute of Applied Chemistry
Chinese Academy of Sciences, Changchun 130022 (China)

Supporting information for this article is available on the WWW under http://www.chemeurj.org/ or from the author.

view, VSB-5 has no essential differences to other Ni catalysts.[9] After activation, Ni^{II} in VSB-5 has been reduced to Ni^0, which takes part in the reactions. Paul et al. investigated hydrogen adsorption at 77 K of VSB-5 in comparison with VSB-1, which showed the existence of coordinatively unsaturated Ni^{2+} sites accessible to H_2 molecules in the pores of VSB-5.[10] Jhung et al. studied isomorphous substitution of transition metal ions[11] in nanoporous VSB-5, and such substituted sites may impart important redox and catalytic properties. Gao et al. assembled Ag[12] and CdS[13] nanoarrays in the porous channels of VSB-5, in attempts to obtain multifunctional catalysts with novel properties. Jhung et al. used VSB-5 as a shape selective catalyst for epoxidation of cyclic olefins with hydrogen peroxide.[14] Nevertheless, little research on the catalytic activity of Ni^{II} in unreduced VSB-5 in selective hydrogenation of nitro compounds and α,β-unsaturated aldehydes has been reported until now. Thus, exploring the catalytic properties of Ni^{II} in VSB-5, which would have a completely different catalytic mechanism for selective hydrogenation, should have great significance for the emergence of new kinds of catalysts.

Reported methods for the preparation of VSB-5 are hydrothermal synthesis at 180 °C for 5 days with organic diamines as templates and microwave irradiation at 180 °C for 4 h with inorganic bases.[15,16] Both synthetic methods can produce VSB-5 materials with a morphology of disordered microrods. Until now, controllable synthesis of VSB-5 with different morphologies and sizes has rarely been reported.[17] Both shape and size control play significant roles in the fabrication of nanoscale catalytic devices for wider use of this nanoporous material.[18,19,20] Furthermore, the exact growth mechanism of VSB-5 is yet to be fully understood.

Here we report a facile hydrothermal approach for producing VSB-5 microspheres assembled from nanorods with control of the precipitation rate of α-$Ni(OH)_2$ and rate of reduction of HPO_2^- to PO_4^{3-} at 140 °C for about 6 h by using HMT as structure-directing agent and NaH_2PO_2 as reducing agent and phosphorus source. Simply by adjusting the pH value of the reaction solution, VSB-5 microspheres assembled from wires and rods with different ranges of diameters and aspect ratios can be obtained conveniently. The growth mechanism of the VSB-5 microspheres was investigated. In addition, the catalytic activity of this material in selective hydrogenation of organic compounds such as styrene, nitrobenzene (NB), *trans*-cinnamaldehyde (CAL), 3-methylcrotonaldehyde (MCA), and 2-chloronitrobenzene (2-CNB) was studied.

Results and Discussion

Controllable synthesis of VSB-5 microspheres assembled from nanowires and rods

Effect of reaction time: Figure 1 shows the X-ray diffraction (XRD) patterns of the as-prepared products obtained at 140 °C and pH 5.58 with the same

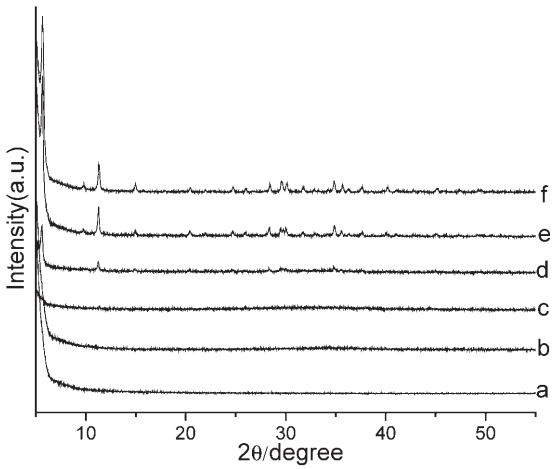

Figure 1. XRD patterns of the products obtained after reactions at 140 °C for different reaction times and molar ratio 1:10:15. a) 1, b) 2, c) 3, d) 4, e) 5, and f) 6 h.

$NiCl_2{\cdot}6H_2O$:HMT:$NaH_2PO_2{\cdot}H_2O$ molar ratio (MR) of 1:10:15 for different reaction times. As the reaction time increased from 1 to 6 h, the crystallinity of the product improved. All peaks in Figure 1 d–f can be readily indexed as those of typical VSB-5 phase reported previously. [8] The X-ray fluorescence (XRF) data (Table 1) provide further confirmation. The Ni:P atomic ratio of 1.69 is almost the same as that of 1.67 reported by Park et al.[8] The presence of C and N in the product may be due to incompletely decomposed product $Ni(OH)_{2-x}(A^{n-})_{x/n}(HMT)_y{\cdot}z{\cdot}H_2O$ ($A = PO_4^{3-}$, HPO_4^{2-}, HPO_2^-).[21]

Table 1. XRF data of VSB-5.

Element	Weight %	Atom %
Ni	70.03	47.95
P	21.86	28.35
C	2.06	6.90
N	5.56	15.94
Na	0.49	0.86
total	100	100

The growth process of these structures in the closed autoclave was carefully monitored by time-dependent experiments. The XRD patterns in Figure 1 and FESEM images in Figure 2 clearly reflect the transformation process of the microspheres. Initially, many aggregates linked like necklaces were present in the products (Figure 2 A), which the XRD pattern confirmed to be amorphous (Figure 1 a). After reaction for 2 h, the surfaces of the necklace-like aggregates became coarse and bushy (Figure 2 B). After 3 h, the product consisted of disperse VSB-5 rods and numerous flower-like microspheres assembled from thin films, which could be identified as α-$Ni(OH)_2$ (Figure 2 C).[21] The images in Figure 2 D and E suggest that the preformed α-$Ni(OH)_2$ acted as a sacrificial template for the formation of VSB-5 microspheres. On further reaction, more and more VSB-5 wires

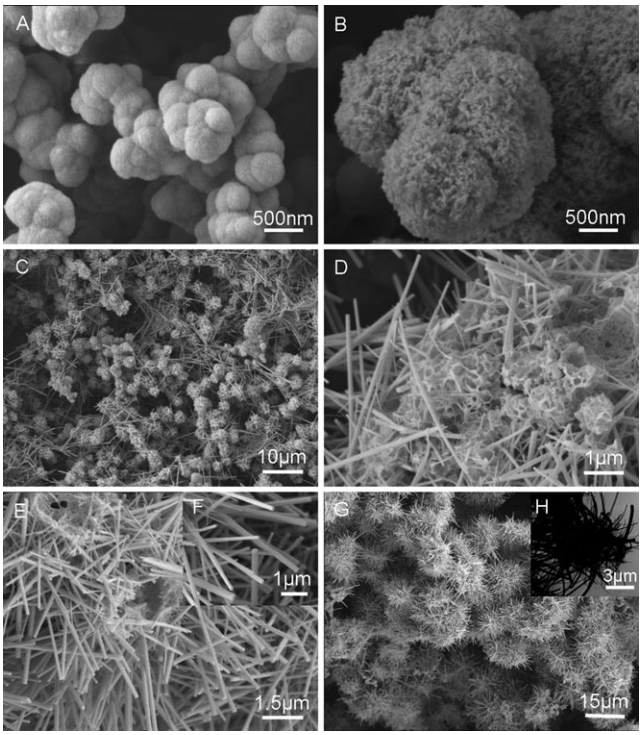

Figure 2. FESEM images of products prepared at 140 °C and MR = 1:10:15 for different reaction times. A) 1, B) 2, C) 3, D), E) 5, and G) 6 h, F) magnified view of G), H) TEM image of the sample shown in G).

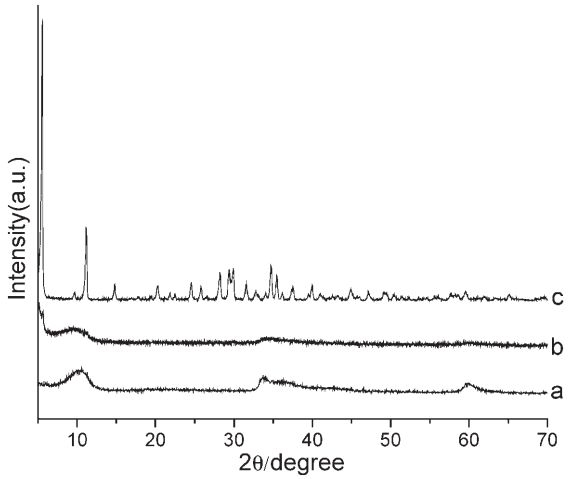

Figure 3. XRD patterns of products prepared at 140 °C for 6 h with different molar ratio. a) 1:10:5, b) 1:10:8, and c) 1:10:15.

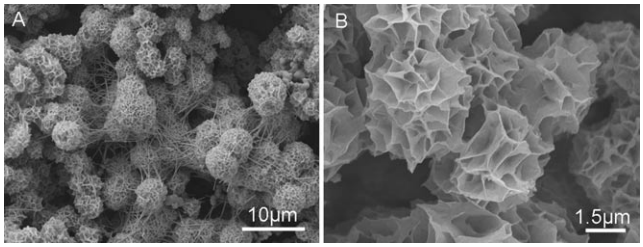

Figure 4. FESEM images of products prepared at 140 °C for 6 h with different molar ratio. A) 1:10:8 and B) 1:10:5.

were observed in the product, and microspheres assembled from wires gradually formed (Figure 2G).

The general overview FESEM image in Figure 2G shows that the product consists of relatively uniform urchinlike microspheres with an average size of 10–17 μm assembled from many hexagonal wires with an average diameter of 195 nm and lengths of up to 17 μm. From the transmission electron microscopy (TEM) image in Figure 2H, the wires did not grow from one core while just overlapping together. During TEM observations, the relatively long exposure of the sample to the electron beam leads to destruction of the microspheres, accompanied by formation of amorphous bent rods.

Effect of the amount of $NaH_2PO_2{\cdot}H_2O$: The influence of the amount of $NaH_2PO_2{\cdot}H_2O$ on the phase transformation was investigated (Figures 3 and 4). When the amount of $NaH_2PO_2{\cdot}H_2O$ was kept at 5 mmol in the reaction system, the product became completely α-$Ni(OH)_2$, as could be confirmed by the corresponding XRD pattern in Figure 3a (JCPDS 38-0715), and flowerlike α-$Ni(OH)_2$ spheres constructed from nanosheets were observed (Figure 4B). A mixture of VSB-5 and α-$Ni(OH)_2$ was obtained when the amount of $NaH_2PO_2{\cdot}H_2O$ increased to 8 mmol (Figure 3b, Figure 4A). When the amount of $NaH_2PO_2{\cdot}H_2O$ was increased to 15 mmol, the resultant product was pure VSB-5 with urchinlike microspherical shape, as shown in Figure 2G. Thus, suitable amounts of $NaH_2PO_2{\cdot}H_2O$ and HMT are essential for formation of the VSB-5 microspheres.

Effect of pH: The influence of the pH value on the final products was investigated. Reactions that took place outside the pH range of 4.2 to 9.0 did not form VSB-5. Figure 5 illustrates that the shape of VSB-5 is strongly dependent on pH. With increasing pH, the morphology of VSB-5 changes from disperse rods, through urchinlike microspheres assembled from wires, to a large number of fibers. Thus, pH value is another key parameter for formation of VSB-5 microspheres. Moreover, it is vital for manipulating the diameters and aspect ratios of the final products. When the initial pH of the reactant solution was adjusted to as low as 4.21 before introduction into the autoclave, homogeneous short rods with well-defined hexagonal-prismatic shape (Sample A) with an average diameter of 800 nm and aspect ratio of about 15 were obtained (Figure 5A and inset). With increasing pH, the diameter decreased and the aspect ratio increased. For example, the product obtained at pH 8.1 is composed of a majority of rods with a diameter of 140 nm (Figure 5E, see also Figure S1 in the Supporting Information). At pH 9.0, the diameter decreased to about 120 nm and the aspect ratio of the VSB-5 fibers increased to 100 or more (Figure 5F). Detailed data are listed in Table 2. This phenomenon could be explained rationally by a series of

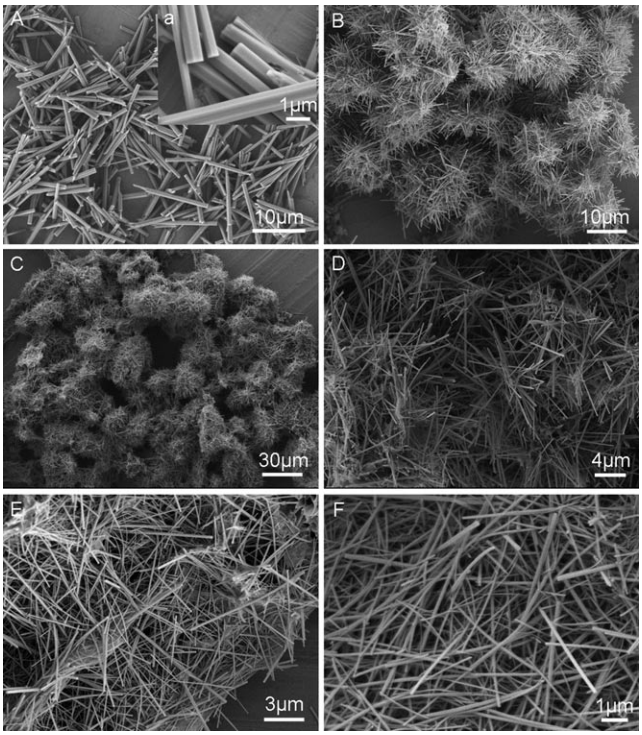

Figure 5. FESEM images of products prepared at 140 °C with the molar ratio 1:10:15 at different pH values. A) 4.21, B) 5.58, C) 6.01, D) 7.02, E) 8.10, and F) 9.00.

Table 2. Analytical data of samples prepared at different pH values with other conditions unchanged.

Sample	pH	MR	d_{av} [a] [nm]	A_{BET} [$m^2 g^{-1}$]	Reaction time [h]
A	4.21	1:10:15	800	285.30	17
B	5.58	1:10:15	195	184.44	6
C	6.01	1:10:15	185	204.70	6
D	7.06	1:10:15	175	212.24	8
E	8.10	1:10:15	140	161.652	8
F	9.00	1:10:15	120	122.859	6

[a] Average diameter of most rods.

chemical reactions occurring in this system. The competition of nucleation with growth was always accompanied by a change in pH value in the whole reaction system, which result in such changes in diameter and aspect ratio.

FTIR and thermogravimetric analysis of nanoporous VSB-5: The FTIR spectrum in Figure 6 shows bands at 3443, 3379, 1620, 1461, 1394, 1325, 1104, 1031, 973, 592, 509, 450 cm^{-1}. The wide band at 3443 cm^{-1} is attributed to the ν_{OH} vibration of H-bonded water molecules located in the structure of VSB-5. The bending vibrational mode of the interior water molecules is found at 1620 cm^{-1}. The narrow peak at 3379 cm^{-1} could be assigned to the ν_{NH} vibration. The series of bands at 1461, 1394, 1325 cm^{-1} are characteristic for ν_{CN}. The band at 592 cm^{-1} could be attributed to $\delta_{\text{-O-H}}$. The peaks at 509 and 450 cm^{-1} are assigned to M–O and

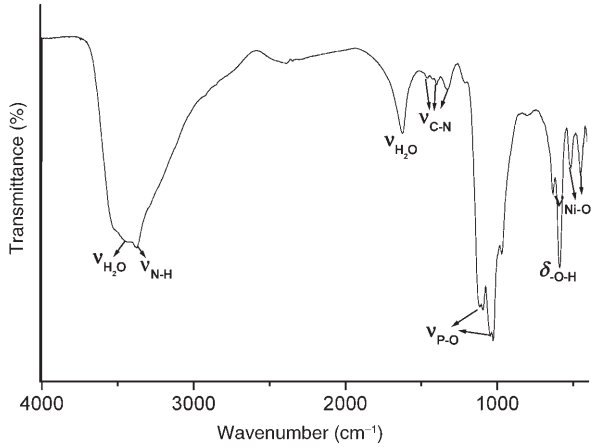

Figure 6. FTIR spectrum of urchinlike VSB-5 microspheres.

M-O-H bending vibrations (ν_{NiO} and $\delta_{Ni\text{-}O\text{-}H}$). The absorptions between 1031 and 592 cm^{-1} are attributed to P–O vibrations of the PO_4 tetrahedra in the VSB-5 structure. The XRF data in Table 1 further confirmed the FTIR data of VSB-5 material.

The thermogravimetry/differential thermal analysis (TG/DTA) plot in Figure 7 shows four steps with distinctive net weight losses of 12.49 (step A, up to 250), 2.17 (step B, 250

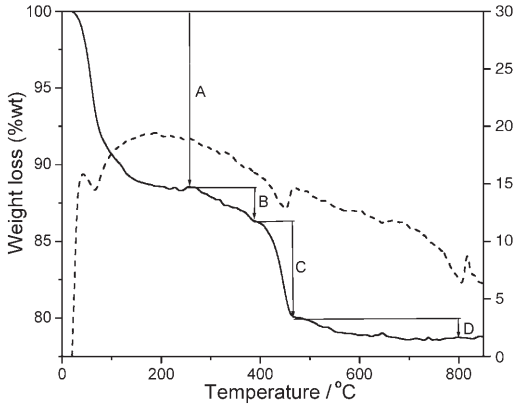

Figure 7. TG/DTA curves of urchinlike VSB-5 microspheres. The dashed line shows the DTA curve in the process.

to 380), 6.26 % wt (step C, from 380 to 460), and 1.36 wt % (step D, from 460 to 800 °C). The total weight loss of 21.28 wt % is a little higher than that reported previously,[8] which could be attributed to the incompletely decomposed product $Ni(OH)_{2-x}(A^{n-})_{x/n}(HMT)_y \cdot z \cdot H_2O$.[22,23] The product after thermogravimetric analysis was examined by XRD, and its pattern could be indexed to that of the condensed $Ni_3(PO_4)_2$ phase (JCPDF Card No. 70-1796; see Figure S2 in the Supporting Information).

BET analysis of nanoporous VSB-5: The BET surface areas of all samples were determined by N_2 adsorption with an ASAP-2020 surface area analyzer (Table 2). Sample A prepared at pH 4.21 has the largest BET surface area (285.3 $m^2 g^{-1}$), most of which is contributed by micropores

(ca. 256.3 m^2g^{-1}). The N_2 adsorption/desorption isotherm and the pore size distribution curve of sample A are shown in Figure 8. Hysteresis of the desorption branch is due to

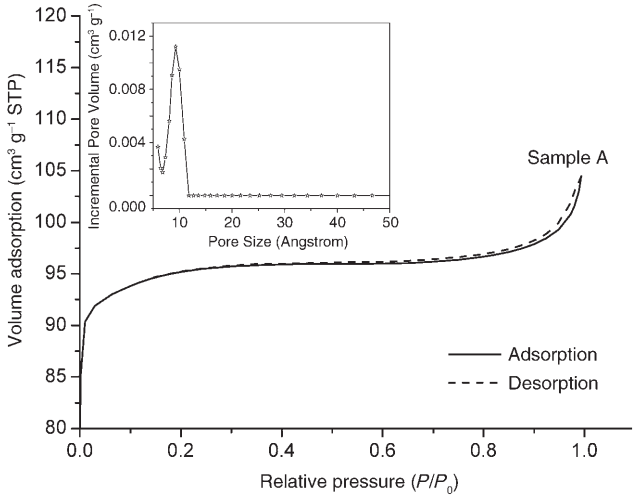

Figure 8. N_2 adsorption/desorption isotherm and pore size distribution (inset) of sample A

hindered desorption, which is often observed in particulate samples.[24] The inset curve of Figure 8 shows that the VSB-5 retained a uniform framework with pore size distribution centered around 0.9 nm, only slightly different from the value of 1.1 nm reported previously.[12,13] From the data in Table 2, it can be concluded that the BET surface area increases with decreasing pH.

Reaction mechanism: The reactions occurring in this system can be described by Equations (1)–(7).

$$(CH_2)_6N_4 + 6\,H_2O \rightarrow 6\,HCHO + 4\,NH_3 \quad (1)$$

$$NH_3 + H_2O \rightarrow NH_4^+ + OH^- \quad (2)$$

$$Ni^{2+} + 2\,OH^- \rightarrow \alpha\text{-}Ni(OH)_2 \quad (3)$$

$$H_2PO_2^- + 2\,HCHO + 2\,H_2O \rightleftharpoons PO_4^{3-} + 2\,HCH_2OH + 2\,H^+ \quad (4)$$

$$PO_4^{3-} + 2\,H^+ \rightarrow H_2PO_4^- \quad (5)$$

$$PO_4^{3-} + H^+ \rightarrow HPO_4^{2-} \quad (6)$$

$$20\,Ni^{2+} + 12\,OH^- + 4\,PO_4^{3-} + 8\,HPO_4^{2-} + 18\,H_2O \rightarrow Ni_{20}[(OH)_{12}(H_2O)_6][(HPO_4)_8(PO_4)_4] \cdot 12\,H_2O \quad (7)$$

Decomposition of HMT could result in several chemical reactions. The resulting products HCHO and NH_3 play different roles in the whole reaction process: HCHO oxidizes $H_2PO_2^-$ to PO_4^{3-}, and NH_3 is the origin of the OH^- in α-$Ni(OH)_2$.[22] From the structural formula of VSB-5, it is clear that the molar ratio of (PO_4^{3-}+HPO_4^{2-}) to OH^- is 1:1. The decomposition of each three HMT molecules will produce 9(PO_4^{3-}+$H_2PO_4^-$+HPO_4^{2-}) and 12 OH^- simultaneously if all the resultant products can be taken advantage of effectively. Hence, an initial excess of OH^- in the system results in the formation of flowerlike α-$Ni(OH)_2$, formed as reported by us previously.[21] The whole reaction process proceeds with accompanying competitive reactions of Ni^{2+} ions with PO_4^{3-} and OH^-. At the beginning, the amount of OH^- is excessive, and its reaction with Ni^{2+} ions dominates. Then abundant OH^-, a small quantity of PO_4^{3-}, and undecomposed HMT react together to form α-$Ni(OH)_2$ hybrid inorganic–organic composites.[21] As the reaction proceeds, the amount of PO_4^{3-} and HPO_4^{2-} increases gradually. Since the thin films with thickness of about 15–50 nm assembled into spinous α-$Ni(OH)_2$ flowers, the surface energy is higher here than elsewhere because of the slender diameter. Hence, these areas are the most easily dissolved and attacked by PO_4^{3-} and HPO_4^{2-} ions. Recrystallization should occur via Ostwald ripening with dissolved Ni^{2+} and OH^- ions from the triple junctions of α-$Ni(OH)_2$ microspheres and enough PO_4^{3-} and HPO_4^{2-} ions in the vicinity growing to VSB-5 nanorods.[25] As the reaction proceeds, α-$Ni(OH)_2$ dissolves gradually and microspheres of VSB-5 assembled from nanorods form simultaneously if enough resultant PO_4^{3-} and HPO_4^{2-} ions are near the α-$Ni(OH)_2$. When the concentrations in the vicinity are too low to produce VSB-5, then the dissolved Ni^{2+} and OH^- would gradually disperse in the whole aqueous solution and react to form unordered VSB-5 rods. This process also accelerates the dissolution rate of α-$Ni(OH)_2$. In acid solution, the equilibrium of Equation (4) evidently shifts to the left. The restricted production rate of PO_4^{3-} ions leads to a decreased nucleation rate of VSB-5, which favors formation of VSB-5 rods with larger diameters, because the nucleation rate is lower than the growth rate. Nevertheless, the reaction time to obtain complete VSB-5 rods was prolonged due to the restraining effect of H^+, which is illustrated clearly in Table 2. In contrast, superlong and much thinner VSB-5 wires were produced on a large scale after a much shorter reaction time. In fact, in the whole growth process of VSB-5, competition between growth and nucleation rates cooperate with the competition between OH^- and PO_4^{3-} ions for reaction with Ni^{2+}. In summary, by controlling the transformation process of relative amounts of OH^- and PO_4^{3-} ions in solution, VSB-5 microspheres assembled from superlong nanowires, which have not been reported so far, and a series of VSB-5 fibers with controlled sizes can be prepared by the present facile hydrothermal method in much shorter time at low temperature.

Catalytic properties of VSB-5 in selective hydrogenation: We tested the catalytic properties of the sample of VSB-5 obtained at pH 4.21 in selective hydrogenation of aromatic nitro compounds and α,β-unsaturated aldehydes [Eqs. (8)–(12)]; the results are summarized in Table 3.

The conversion of styrene to ethylbenzene can reach 17.9 %, and thus Ni^{II} in VSB-5 clearly shows catalytic activi-

Table 3. Results of selective hydrogenations of several unsaturated compounds with VSB-5.[a]

Run	Substrate	Product	Solvent	T [°C]	t [h]	Conversion [%]	Selectivity [%]
1	styrene	ethylbenzene	benzene	40	4	17.9	–
2	CAL	hydrocinnamaldehyde	hexane	60	5	11.5	100
3	MCA	3-methylbutyraldehyde	hexane	50	10	40.6	99.1
4	NB	aniline	ethanol	50	10	6.3	89.8
5	2-CNB	2-chloroaniline	hexane	50	10	14.5	96.6

[a] Reaction conditions: substrate 1 mmol, solvent 2 mL; molar ratio of substrate:VSB-5 50:1; H_2 pressure 5 MPa.

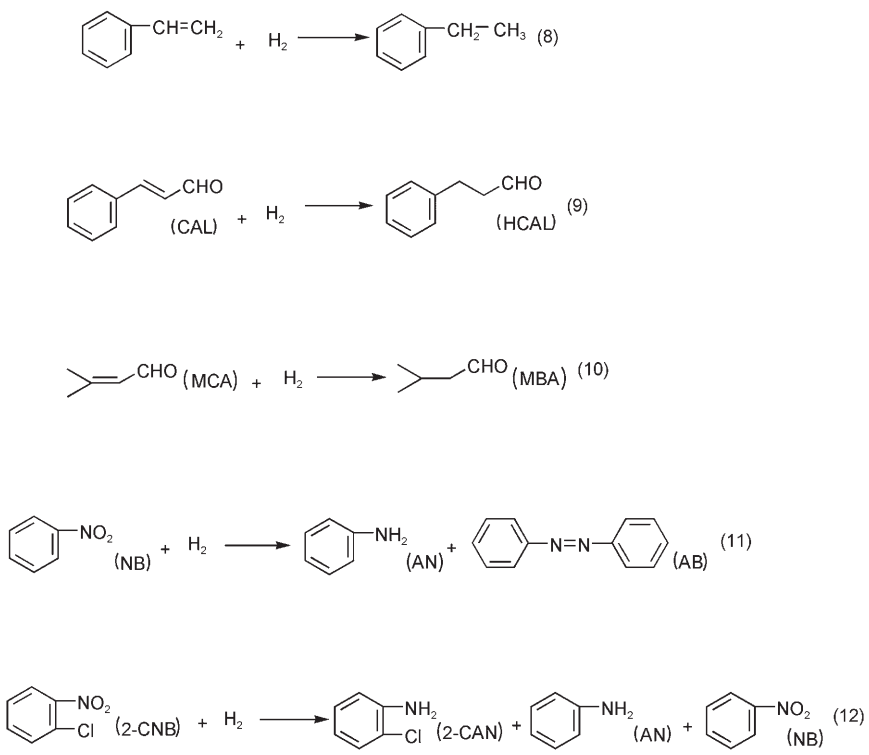

ty in this hydrogenation reaction. Although conversion is low, it is proof of the hydrogenation activity of Ni^{II}, which has rarely been reported until now.

To further examine the catalytic activity of VSB-5 in selective hydrogenation of other functional groups, *trans*-cinnamaldehyde (CAL), 3-methylcrotonaldehyde (MCA), nitrobenzene (NB), and 2-chloronitrobenzene (2-CNB) were chosen. Hydrogenation of the unsaturated aldehydes CAL and MCA gave hydrocinnamaldehyde (HCAL) and 3-methylbutyraldehyde (MBA), respectively. These two reactions prove that VSB-5 can hydrogenate a C=C bond selectively as opposed to the C=O bond in unsaturated aldehydes. Hydrogenation of NB gave aniline with high selectivity (89.8%), while in the reduction of 2-CNB the selectivity for 2-chloroaniline (2-CAN) reached 96.6%. Thus, nearly all of the selected hydrogenation reactions could be performed with VSB-5 catalyst with high selectivity, although it still has the disadvantage of lower catalytic activity. This may be attributable to the 0.9 nm pore size of the VSB-5 prepared here, which may affect diffusion of larger molecules and thus decrease the reaction rate.[26] It has been proposed that for efficient reduction of larger organic molecules, pores with diameters exceeding 1.5 nm are necessary to host the hydrogenation active site and the molecules at the same time.[27]

To investigate the catalytic activity of VSB-5 prepared at different pH values, we chose the selective hydrogenation of 2-CNB (Table 4). The VSB-5 catalysts have high selectivity for 2-CAN regardless of the pH at which they were prepared. Keeping all other catalytic parameters the same as above, we found that alkaline preparation of catalysts seems to be beneficial for the conversion of 2-CNB to 2-CAN. Both catalysts obtained in alkaline solution gave yields of 2-CAN higher than 70.0%, which is unusual for this catalyst. In contrast, conversion was only 14.5, 11.0, and 34.6% for catalysts prepared at pH 4.21, 6.01, and 7.06, respectively. However, a special case was the sample prepared at pH 5.58, for which conversion reached 78.5%, although the reason is still unclear. Despite this, we could conclude that the conversion rate of 2-CNB can be more influenced by preparing catalysts at different pH values than by morphology. Considerable work is still needed to improve the catalytic activity and to explore the exact mechanism of selective hydrogenation with Ni^{II} in VSB-5 prepared under different conditions.

Table 4. Results of selective hydrogenation of 2-CNB with VSB-5 at different pH values

pH value	5.58	6.01	7.06	8.10	9.00
conversion [%]	78.5	11.0	34.6	71.3	72.0
selectivity [%]	98.7	99.1	97.3	98.2	98.6

Conclusion

Large-scale synthesis of nanoporous VSB-5 materials with urchinlike microspherical morphology and controllable

aspect ratios and diameters has been realized by a convenient hydrothermal process in shorter reaction time at low temperature. By controlling the rate of release of Ni^{2+} in a preformed sacrificial template of α-$Ni(OH)_2$, the rate of oxidation of HPO_2^- to PO_4^{3-}, and pH value, urchinlike VSB-5 microspheres can be produced. In addition, VSB-5 microrods with different diameters and urchinlike microspheres assembled from wires can be obtained on a large scale simply by adjusting the pH of the reaction solution. Reaction time, pH value, and ratio of HMT to $NaHPO_2{\cdot}H_2O$ significantly influence the morphology and quality of the final products. The catalytic activity of Ni^{II} in VSB-5 for selective hydrogenation of several unsaturated organic compounds was tested. It could catalyze reduction of nitrobenzene and 2-chloronitrobenzene to aniline and 2-chloroaniline, and also showed relatively high selectivity for hydrogenation of C=C as opposed to C=O in unsaturated aldehydes, which would have potential applications in synthesizing dyes, agrochemicals, pharmaceuticals, and fragrances.

Experimental Section

Chemicals: The following analytical-grade reagents were purchased from the Shanghai Chemical Reagents Company and used without further purification: $NiCl_2{\cdot}6H_2O$, hexamethylenetetramine (HMT, $C_6H_{12}N_4$), $NaHPO_2{\cdot}H_2O$, benzene, hexane, ethanol, styrene, nitrobenzene (NB), *trans*-cinnamaldehyde (CAL), 3-methylcrotonaldehyde (MCA), and 2-chloronitrobenzene (2-CNB).

Synthetic procedures: In a typical procedure, 1 mmol of $NiCl_2{\cdot}6H_2O$, 10 mmol of HMT, and different amounts of $NaHPO_2{\cdot}H_2O$ were added into 25 mL of deionized water with stirring until the solution was clear. Then, HCl (1 M) or $NH_3{\cdot}H_2O$ (1 M) was used to adjust the pH of the solution to the desired value. Then the solution was transferred to a Teflon-lined autoclave with a volume of 35 mL. The autoclave was sealed and maintained at 140 °C for several hours, and then allowed to cool to room temperature. After the reaction, the green or gray-green precipitate was separated from the solution by centrifugation, washed with deionized water and absolute ethanol several times, and dried under vacuum at 60 °C for 4 h. The dried sample was dehydrated at 350 °C for 1 h under vacuum and kept in a closed desiccator. Based on elemental nickel, the final yield of VSB-5 can be as high as 91.4%.

Selective hydrogenation: The reaction was performed in a 50 mL stainless steel autoclave reactor with a magnetic stirrer. A definite quantity of the catalyst, organic precursor, and solvent were put into the reactor under nitrogen atmosphere and the reaction was carried out with continuous stirring at the desired temperature and a hydrogen pressure of 5 MPa). After the reaction, the reaction mixtures were centrifuged and analyzed by gas chromatography with an FID detector (Shimadzu GC-2010) and a chiral capillary column (Rtx@-50, 30 m × 0.25 m × 0.25 μm).

Characterization: The products were characterized by X-ray diffraction pattern, recorded on a MAC Science Co. Ltd. MXP 18 AHF X-ray diffractometer with monochromatized $Cu_{K\alpha}$ radiation ($\lambda = 1.54056$ Å). Transmission electron microscopy (TEM) was performed on a Hitachi (Tokyo, Japan) H-800 transmission electron microscope at an accelerating voltage of 200 kV. FESEM images were taken on a JEOL JSM-6700F field emission scanning electron microscope at 10 kV; the IR spectrum was obtained on a Magna-IR-750 spectrometer; thermogravimetric analysis (TGA) was carried out on a TGA-50H thermal analyzer (Shimadzu Corporation) with a heating rate of 10 °C min^{-1} in flowing air. X-ray fluorescence (XRF) measurements were performed on a XRF-1800 X-ray fluorescence spectrometer (Shimadzu Corporation) at room temperature. N_2 adsorption was determined by BET measurements with an ASAP-2020 surface area analyzer.

Acknowledgements

S.H.Y. acknowledges the special funding support from the National Natural Science Foundation of China(NSFC, Nos. 50732006, 20325104, 20621061, 20671085), the 973 project (2005CB623601), the Centurial Program of the Chinese Academy of Sciences, Anhui Development Fund for Talent Personnel and Anhui Education Committee (2006Z027, ZD2007004-1), the Scientific Research Foundation for the Returned Overseas Chinese Scholars, the Specialized Research Fund for the Doctoral Program (SRFDP) of Higher Education State Education Ministry, and the Partner-Group of the Chinese Academy of Sciences, the Max Planck Society.

[1] V. Kratky, M. Kralik, M. Mecarova, M. Stolcova, L. Zalibera, *Appl. Catal. A Gen.* **2002**, *235*, 225.
[2] F. Y. Zhao, Y. Ikushima, M. Arai, *J. Catal.* **2004**, *224*, 479.
[3] R. X. Liu, F. Y. Zhao, S. I. Fujita, M. Arai, *Appl. Catal. A: Gen.* **2007**, *316*, 127.
[4] M. Chatterjee, Y. Ikushima, F. Y. Zhao, *New J. Chem.* **2002**, *26*, 510.
[5] a) N. Thakar, R. J. Berger, F. Kapteijn, J. A. Moulijn, *Chem. Eng. Sci.* **2007**, *62*, 5322; b) N. Semagina, A. Renken, L. K. Minsker, *Chem. Eng. Sci.* **2007**, *62*, 5344; c) Á. Mastailir, B. Rác, Z. Király, Á. Molnár, *Catal. Commun.* **2008**, in press.
[6] a) P. Kukula, V. Gabova, K. Koprivova, *Catal. Today* **2007**, *121*, 27; b) E. A. Nieto, B. B. Baeza, A. G. Ruiz, R. Ramos, *Appl. Catal. A* **2006**, *303*, 88.
[7] a) B. M. Reddy, G. M. Kumar, I. Ganesh, *J. Mol. Catal. A* **2006**, *247*, 80; b) B. M. Reddy, G. K. Reddy, K. N. Rao, *J. Mol. Catal. A* **2007**, *265*, 276; c) H. X. Li, Y. D. Wu, Y. Wan, *J. Catal. Today.* **2004**, *94*, 493; d) S. J. Chiang, B. J. Liaw, Y. Z. Chen, *Appl. Catal. A* **2007**, *319*, 144.
[8] N. Guillou, Q. Gao, P. M. Forster, J. S. Chang, M. Nogues, S. E. Park, G. Ferey, A. K. Cheetham, *Angew. Chem.* **2001**, *113*, 2913; *Angew. Chem. Int. Ed.* **2001**, *40*, 2831.
[9] V. F. D. Álvaro, R. A. W. Johnstone, *J. Mol. Catal. A* **2008**, *280*, 131.
[10] P. M. Forster, J. Eckert, J. S. Chang, S. E. Park, G. Ferey, A. K. Cheetham, *J. Am. Chem. Soc.* **2003**, *125*, 1309.
[11] S. H. Jhung, J. S. Chang, Y. K. Hwang, J. M. Greneche, G. Ferey, A. K. Cheetham, *J. Phys. Chem. A J. Phys. Chem. B.* **2005**, *109*, 845.
[12] Z. Chen, Q. M. Gao, D. M. Gao, Q. Y. Wei, M. L. Ruan, *Mater. Lett.* **2006**, *60*, 1816.
[13] D. L. Jian, Q. M. Gao, D. M. Gao, M. L. Ruan, W. Shi, *Phys. Lett. A* **2006**, *357*, 136.
[14] S. H. Jhung, J. H. Lee, A. K. Cheetham, *J. Catal.* **2006**, *239*, 97.
[15] S. H. Jhung, J. H. Lee, P. M. Forster, G. Ferey, A. K. Cheetham, J. S. Chang, *Chem. Eur. J.* **2006**, *12*, 7899.
[16] S. H. Jhung, J. W. Yoon, J. S. Hwang, A. K. Cheetham, J. S. Chang, *Chem. Mater.* **2005**, *17*, 4455.
[17] S. H. Jhung, J. W. Yoon, Y. K. Hwang, J. S. Chang, *Microporous Mesoporous Mater.* **2006**, *89*, 9.
[18] Y. W. Jun, M. F. Casula, J. H. Sim, S. Y. Kim, J. Cheon, A. P. Alivisatos, *J. Am. Chem. Soc.* **2003**, *125*, 15981.
[19] Y. W. Jun, J. S. Choi, J. Cheon, *Angew. Chem.* **2006**, *118*, 3492; *Angew. Chem. Int. Ed.* **2006**, *45*, 3414.
[20] W. T. Yao, S. H. Yu, S. J. Liu, J. P. Chen, X. M. Liu, F. Q. Li, *J. Phys. Chem. B.* **2006**, *110*, 11704.
[21] B. H. Liu, S. H. Yu, S. F. Chen, C. Y. Wu, *J. Phys. Chem. B.* **2006**, *110*, 4039.
[22] Z. B. Huang, Y. Zhu, S. T. Wang, G. F. Yin, *Cryst. Growth Des.* **2006**, *6*, 1931.
[23] Q. C. Li, V. Kumar, Y. Li, H. T. Zhang, T. J. Marks, R. P. H. Chang, *Chem. Mater.* **2005**, *17*, 1001.

[24] a) Z. Wang, J. M. Heising, A. Clearfield, *J. Am. Chem. Soc.* **2003**, *125*, 10375; b) A. Subbia, D. Pyle, A. Rowland, J. Huang, R. A. Narayanan, P. Thiyagarajan, J. Zon, A. Clearfield, *J. Am. Chem. Soc.* **2005**, *127*, 10826.

[25] a) Y. G. Sun, B. Mayers, Y. N. Xia, *Nano Lett.* **2003**, *3*, 675; b) Y. G. Sun, B. Mayers, T. Herricks, Y. N. Xia, *Nano Lett.* **2003**, *3*, 955; c) Z. Y. Tang, N. A. Kotov, M. Giersig, *Science* **2002**, *297*, 237; d) Y. G. Sun, Y. D. Yin, B. T. Mayers, T. Herricks, Y. N. Xia, *Chem. Mater.* **2002**, *14*, 4736; e) Z. A. Peng, X. G. Peng, *J. Am. Chem. Soc.* **2001**, *123*, 1389.

[26] a) H. J. Zhang, X. C. Meng, Y. D. Li, *Ind. Eng. Chem. Res.* **2007**, *46*, 4186; b) K. M. Reddy, C. Song, *Catal. Today* **1996**, *31*, 137; c) S. Albertazzi, E. Rodri′guez-Castello′n, M. Livi, A. Jime′nez-Lo′pez, Vaccari, *J. Catal.* **2004**, *228*, 218; d) B. M. Choudary, K. M. Lakshmi, R. N. Mahender, *Appl. Catal. A* **1999**, *181*, 139.

[27] X. C. Meng, Y. X. Wu, Y. D. Li, *J. Porous Mater.* **2006**, *13*, 365.

Received: November 21, 2007
Published online: March 11, 2008

